Isı Bilimi ve Tekniği Dergisi, 40, 2, 221-235, 2020
J. of Thermal Science and Technology

ISSN 1300-3615
https://doi.org/10.47480/isibted.816994

INVESTIGATION OF THE TIME DEPENDENT THERMAL BEHAVIOR OF A CONTAINER WITH PCM WALLS DURING A HOT SUMMER DAY

Çiğdem SUSANTEZ* and Aldélio Bueno CALDEIRA**
*Trakya University, Engineering Faculty, Mechanical Engineering Department, Edirne - 22030, Turkey, cigdemsusantez@trakya.edu.tr, ORCID: 0000-0002-2449-2551
**Department of Mechanical and Materials Engineering, Military Institute of Engineering, Rio de Janeiro - 22290-270, Brazil, aldelio@ime.eb.br, ORCID: 0000-0002-7261-9924

(Geliş Tarihi: 05.01.2020, Kabul Tarihi: 10.05.2020)

Abstract: In this paper, the thermal comfort of a container with PCM walls has been investigated numerically for a hot summer day in Rio de Janeiro. Four different cases have been investigated. These cases are: *(i)* container made by Polyurethane plates, which is the reference solution, *(ii)* RT 22 HC plates, *(iii)* RT 25 HC plates and *(iv)* RT 28 HC plates. Analyses have been performed for 10 hours from 08:00 to 18:00 h, and dimensionless numerical results for all investigated cases have been presented. Nondimensional governing equations have been solved by COMSOL Multiphysics finite element modeling and simulation software. Results show that although thermal conductivity of polyurethane is one-eighth of that of PCM, the container with PCM walls present considerably better performance. It has been observed that the average value of the dimensionless temperature inside the container is equal to its initial value at the end of the investigation time for the cases of RT 22 HC and RT 25 HC are used. On the other hand, this value shows increments of 0.1235 (2.35ºC) and 0.7710 (14.65ºC) respect to initial temperature, respectively for the cases of RT 28 HC and polyurethane are used at the end of that time.
Keywords: Phase change material, Buoyancy, Thermal comfort, Container

SICAK BİR YAZ GÜNÜNDE FDM DUVARLI KONTEYNERİN ISIL DAVRANIŞININ İNCELENMESİ

Özet: Bu çalışmada, FDM duvarlı konteynerin ısıl konforu Rio de Janeiro'da sıcak bir yaz günü şartlarında nümerik olarak incelenmiştir. *(i)* Poliüretan plakalardan (referans olarak incelenen durum), *(ii)* RT 22 HC, *(iii)* RT 25 HC ve *(iv)* RT 28 HC plakalarından olmak üzere dört farklı durum incelenmiştir. Analizler saat 08:00'dan saat 18:00'a kadar olmak üzere 10 saat için yapılmış ve boyutsuz nümerik sonuçlar incelenen her durum için COMSOL Multiphysics sonlu elemanlar modelleme ve simülasyon yazılımıyla elde edilerek sunulmuştur. Poliüretanın ısıl iletkenliği FDM'nin ısıl iletkenliğinin sekizde biri olmasına rağmen, FDM duvarlı konteynerin daha iyi performans gösterdiği görülmüştür. Analiz zamanı sonunda konteyner içindeki boyutsuz ortalama sıcaklık değerinin RT 22 HC ve RT 25 HC'nin kullanıldığı durumlarda başlangıç değerine eşit olduğu görülmüştür. Diğer yandan, RT 28 HC ve poliüretanın kullanıldığı durumlarda bu değerin, söz konusu süre sonunda başlangıç sıcaklığına göre sırasıyla 0.1235 (2.35ºC) ve 0.7710 (14.65ºC) artış gösterdiği sonucuna ulaşılmıştır.
Anahtar kelimeler: Faz değiştiren malzeme, Kaldırma kuvveti, Isıl konfor, Konteyner

NOMENCLATURE

A^*: Dimensionless area
Bi: Biot number
c: Specific heat [J/kgK]
C: Heat capacity [J/K]
c_p: Specific heat at constant pressure [J/kgK]
$\vec{g}$: Gravitational acceleration [m/s^2]
H: Height of the container [m]
h_{out}: Convection coefficient outside the container [W/m^2 K]
k: Thermal conductivity [W/mK]
L: Width of the container [m]
L_x: Length of the square enclosure [m]
L_z: Length of the container along the z-axis [m]
$\overline{Nu}_L$: Nusselt number [$\overline{Nu}_L = \frac{h_{out}L_z}{k_f}$]
$\vec{n}$: Unit normal vector
n: Length in the normal direction
Pr: Prandtl number [$Pr = \frac{\gamma_f}{\alpha_f}$]
p: Pressure [Pa]
R^2: Coefficient of determination
Re_L: Reynolds number [$Re_L = \frac{wL_z}{\gamma_f}$]
Ra: Rayleigh number [$Ra = \frac{g\beta_T L^3 (T_H - T_0)}{\alpha_f \gamma_f}$]
Ste: Stefan number [$Ste = \frac{c_l(T_l - T_s)}{\Delta h}$]
S^*: Dimensionless length in the horizontal direction
T: Temperature [ºC]
T_H: Maximum value of the outside air temperature [ºC]
T_l: Liquefication temperature [ºC]

T_{out}: Air temperature outside of the container
T_{ref}: Reference temperature (Minimum temperature in the domain of air) [^{o}C]
T_s: Solidification temperature [^{o}C]
t: Time [s]
t_m: Thickness of the container walls [m]
u: Velocity along with the x-axis [m/s]
$\vec{V}$: Velocity vector [m/s]
$V^*{}_{max}$: Maximum value of the dimensionless velocity
v: Velocity with along the y-axis [m/s]
w: Velocity with along the z-axis [m/s]
x, y, z: Horizontal, vertical and perpendicular coordinates [m]

Greek Symbols

α: Thermal diffusivity [m^2/s]
β : Melt fraction
β_T: Thermal expansion coefficient of air [K^{-1}]
Δh: Latent heat [J/kg]
ρ: Density [kg/m^3]
μ: Dynamic viscosity [kg/ms]
γ: Kinematic viscosity [m^2/s]
θ: Dimensionless temperature used in the validation

Subscript

0: Initial
ave: Average
B: Bottom
c: Cold
ap: Apparent
f: Fluid
h: Hot
l: Liquid phase
max: Maximum
min: Minimum
s: Solid-phase
PCM: Phase change material
pol: Polyurethane
S: Side
T: Top

Superscript

*: Shows the dimensionless quantities

Abbreviations

PCM: Phase change material

INTRODUCTION

Phase change materials (PCMs) have been used in many engineering fields such as thermal protection of foods and electronic devices, thermal storage of solar energy, cooling of engines, thermal comfort in vehicles, medical applications and spacecraft thermal systems (Zalba *et al.*, 2003; Rubitherm, 2019a; Shobo *et al.*, 2018). Most of the PCMs used in industry are impure substances. Although in the case of pure substance phase change occurs at a constant temperature, small temperature variation could be observed during the phase change of impure substances. When PCM reaches its solidification temperature, T_s, melting starts, and the phase change continues by absorbing more heat from its surroundings until it reaches to the liquefication temperature, T_l. On the other hand, PCMs make a heating effect by releasing heat they stored when they are solidifying.

There are many studies about building applications of PCMs. Alvare *et al*. (2013) proposed new designs for the PCM cooling unit, improving the utilization factor, increasing the convective heat transfer coefficient, and the contact area between PCM and air. Beltran *et al*. (2019) conducted a study on the selection of PCM for building wallboards and roofs. In their study, they used multicriteria decision methods on a reference house designed in Ecuador with 36 m^2 in space. According to their results, the best PCMs were n-Octadecane and BioPCM-Q29. Cheng *et al*. (2015) used heat conduction-enhanced shape-stabilized PCM (HCE-SSPCM) with an underfloor heating system. They charged this system with electricity at night when electricity is cheap. They obtained the result that the energy efficiency of the heating system can be improved, and the thickness of the thermal insulation material can be reduced by enhancing the thermal conductivity of PCM. They also showed that when thermal conductivity is smaller than 1 W/mK, this improving effect is not obvious. Chou *et al*. (2013) proposed a new design for metal sheet roofing structure in order to absorb more heat by solar radiation during the day in their experimental and numerical study. They obtained the result that this new design can reduce the heat flow through the roof significantly. Derradji *et al*. (2017) used TRNSYS 17 software to compare the thermal behavior of an office in Algeria having conventional walls with another office whose walls incorporated with PCM. According to their results, the use of PCM into walls not only increased the office temperature by 3 to 4^{o}C in the winter period but also decreased it by 7^{o}C the in summer period. Elargo *et al*. (2017) made an experimental and numerical study on the thermal performance of PCM integrated into a roof space in Italy. They showed that the heat peak load is reduced between 13% to 59% depending on the type of PCM. Gracia *et al*. (2013) experimentally investigated the thermal performance of the ventilated facade with PCM in its air cavity. They performed their tests on two identical cubicles in Spain, and one of them has a ventilated facade. They made different systems for night free cooling applications, cold storage units, and overheating protection systems by using gates at the different openings of the channel. They obtained the result that the most promising one for reducing the cooling load of the cubicle is the night free cooling application. Kharbouch *et al*. (2017) applied an optimization method by coupling the Genopt optimization tool and EnergyPlus building simulation tool to minimize the heating and cooling load of an air-conditioned house with PCMs in north Moroccan. They presented the optimum parameters for the orientation of the house, PCM layer thickness, rate of glazing area, glazing window type, air infiltration rate, solar absorptance coefficient of the outside surface of the external wall, and PCM melting temperature. According to their study, the optimum value of the PCM melting temperature is 20^{o}C. Meng *et al*. (2017) made an experimental and numerical study on the concept of a composite PCM room consisting of two PCMs with different melting temperatures. They performed their

analysis in winter and summer conditions and obtained the results that the temperature drop of the PCM room was about 4.28-7.7ºC during the summer day, the temperature rise of that was about 6.93-9.48ºC during the winter day when comparing to an ordinary room. Stritih *et al*. (2018) performed an analysis of the composite wall filled with different PCMs by using TRNSYS software. They showed that the walls with PCMs could reduce the energy usage of the building. Xia *et al*. (2017) numerically investigated the heat transfer of the PCM wall by using the sensible heat capacity method. They concluded the result that the melting temperature of the PCM should be close to the indoor air temperature to reduce the heat transfer from the PCM wall to the room. They also showed that the latent heat of the PCM has not a significant effect on the inner surface heat flux. Hichem *et al*. (2013) made an experimental and numerical study on the thermal behavior of brick, some of whose square holes were filled with PCM. According to their results, using brick with PCM in this way not only reduces the temperature of the inner wall up to 3.8ºC but also the entering heat flux up to 82.1%. Ye *et al*. (2017) experimentally and numerically investigated the thermal performance of PCM panels for building applications. They found that the optimum thickness of the PCM panel is about 8-10mm. They also underlined that CaCl2.6H2O/expanded graphite panels exhibit better thermal performance than that of RT27/expanded graphite panels. Wang *et al*. (2013) numerically investigated the thermal performance of the ultrathin envelope integrated with PCM in Chengdu, China. They suggested that the thermal conductivity coefficient of PCM should be small, its latent heat should be high, phase transition temperature range should be narrow, and the PCM should be located at the inner side for better performance. Li *et al*. (2019) made a numerical study on the thermal performance of the Trombe wall integrated with double layers of PCM in Wuhan. They concluded that the PCM Trombe wall causes a lower indoor temperature in summer and reduces indoor temperature fluctuations in winter.

On the other hand, energy saving is an important factor for living units. Arce *et al.* (2020) have simulated the effects of three PCM configurations in the structure of a container, considering the ambient conditions of three cities in the USA and three cities in Spain. These cities are Abiline, Albuquerque, Barstow, Cordoba, Tenerife, and Yuma. Moreover, the influence of carbon nanofibers and boron nitride particles inside the PCM material was investigated, since these materials enhance the heat transfer. The results have shown that 23% of energy savings can be reached by using PCM materials. In addition, the suited case with carbon nanofibers was better than the ones with boron nitride in relation to energy saving. Park *et al.* (2019) were devoted to investigating the temporary modular housing for use in disasters and containers. Simulations were performed in order to evaluate the heating/cooling and photovoltaic energy generation. Eight types of modular houses were studied, and the thermal analyses of heating and cooling loads have considered the following places: Bangkok, Dacca, Chengdu, Ulsan, and Sapporo. The results have shown that airtightness is a serious problem, which must be overcome to satisfy the standards and it has a relevant influence on the heating and cooling loads. Udosen *et al.* (2019) have simulated the heat transfer in a container house with high-density polyethylene-PCM capsules in the structure. The transient one-dimensional numerical model was implemented in MATLAB, adopting explicit first-order finite difference and the effective heat capacity methods. The results have indicated that the proposed approach can reduce the indoor temperature of the container up to 10.2ºC. Nevertheless, better results can be reached if fans were placed in strategic locations to improve the airflow inside the house and remove the hot air from the container. Hu *et al.* (2020) have investigated the PCM applied in a ventilated window. The experiments have employed paraffin wax 50% with fiberboard, and fans were used to control the forced convection. Experiments with a reference window without PCM was also performed in order to evaluate the PCM efficiency. The results have shown that the PCM, exploring the heating process, can increase the inlet air temperature by 2.0°C, while in self-cooling mode can reduce the glass surface temperature by an average of 0.8°C.

This study presents the effects of the three types of convenient PCM container walls on thermal comfort for the climatic conditions of Rio de Janeiro. In this study, for that purpose, the thermal comfort of a container with PCMs for a hot summer day in Rio de Janeiro has been investigated numerically. The model consisting of governing equations for air and PCM has been proposed, and corresponding governing equations have been solved. Nondimensionalized governing equations have been solved by COMSOL Multiphysics finite element modeling and simulation software, and thermal performances of three different PCMs have been presented. This study not only shows the preference of convenient PCM materials to the usual isolation materials like polyurethane due to the latent heat of PCMs but also enables comparison between PCMs by considering the thermal comfort of a container during a hot summer day in Rio de Janeiro.

MATERIAL AND METHOD

Problem and Proposed Mathematical Model

In this study container designed with PCM walls was investigated to prevent the container from the hot outside air. The container, a closed enclosure, has a canopy above to prevent solar radiation, and it is subjected to airflow in the *z*-direction, as shown in Fig.1. The effect of the implementation of three types of PCM embedded wall and polyurethane wall on the indoor air temperature of the container have been investigated. Analyses have been performed for two-dimensional axial symmetric conditions, as seen in Fig. 2.

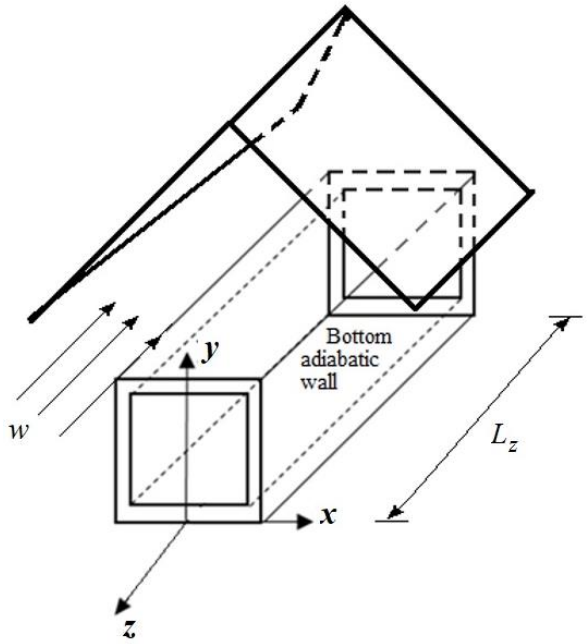

Fig. 1 Container design

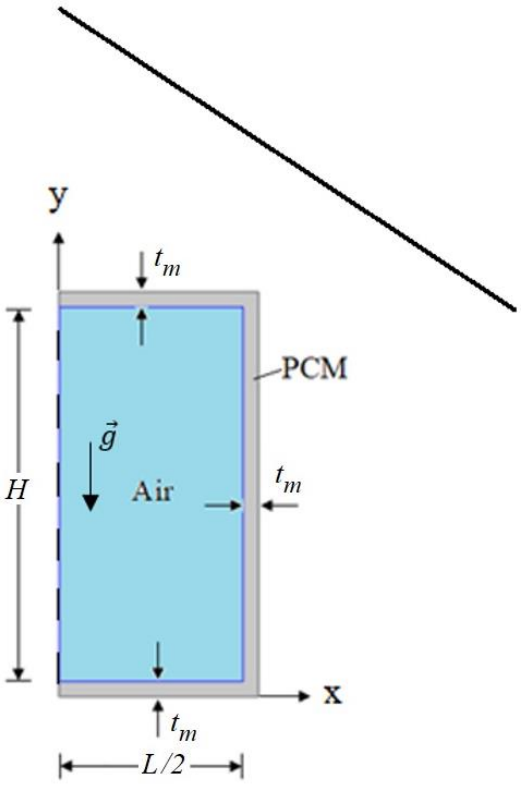

Fig. 2 Investigated domain

Geometric dimensions and thermophysical properties of the related materials are given in Table 1 and Table 2, respectively. The thermophysical properties of air are taken at 25ºC, and assumed to be constant. The thermophysical properties of investigated PCMs are given in Table 3.

Table 1 Geometric dimensions

$t_m = 0.1$ m	
$H = 2.4638$ m (8 feet 1 inch)	(Ulloa *et al.*, 2017)
$L = 2.4384$ m (8 feet)	(Ulloa *et al.*, 2017)
$L_z = 6$ m	

Table 2 Thermophysical properties

$\rho_f = 1.184$ kg/m^3	(Çengel and Cimbala, 2005)
$c_{pf} = 1007$ J/kg K	(Çengel and Cimbala, 2005)
$k_f = 0.02551$ W/mK	(Çengel and Cimbala, 2005)
$\mu_f = 0.00001849$ kg/ms	(Çengel and Cimbala, 2005)
$Pr = 0.7296$	(Çengel and Cimbala, 2005)
$\rho_{pol} = 30$ kg/m^3	(BING, 2019)
$c_{pol} = 1500$ J/kg K	(BING, 2019)
$k_{pol} = 0.025$ W/m K	(BING, 2019)

Table 3 Thermophysical properties of PCMs (Rubitherm, 2019b)

PCM	T_s (ºC)	T_l (ºC)	$c_s = c_l$ (J/kgK)	ρ_s (kg/m^3)	ρ_l (kg/m^3)	$k_s = k_l$ (W/mK)	Δh (kJ/kg)
RT 28 HC	27	29	2000	880	770	0.2	220
RT 25 HC	22	26	2000	880	770	0.2	200
RT 22 HC	20	23	2000	760	700	0.2	160

Natural convection causes fluid motion inside the container. Initial and boundary conditions for the study have been presented in equations (1)-(7). Solar radiation has been neglected due to the canopy above the container. Its effect is also small when comparing heat transfer due to forced convection outside the container. The face of the container, which is in contact with the ground, is assumed to be adiabatic.

$$T|_{t=0} = T_0 \tag{1}$$

$$\left.\frac{\partial T}{\partial y}\right|_{y=0} = 0 \tag{2}$$

$$u|_{on\ walls} = 0 \qquad v|_{on\ walls} = 0 \tag{3}$$

$$k_f \frac{\partial T}{\partial n} = k_i \frac{\partial T}{\partial n} \quad \text{Inside boundary condition} \tag{4}$$

$$h_{out}(T - T_{out}) = -k_i \frac{\partial T}{\partial n} \quad \text{Outside boundary condition} \tag{5}$$

i refers to PCM or polyurethane

$$\left.\frac{\partial T}{\partial x}\right|_{x=0} = 0 \qquad \text{Symmetry condition for the energy equation} \qquad (6)$$

$$\left.\vec{V}\cdot\vec{n}\right|_{x=0} = 0 \qquad \text{Symmetry condition for momentum equations} \qquad (7)$$

Assumptions:
- The bottom surface of the container is adiabatic.
- Thermophysical properties are constant.
- Thermal radiation is neglected because of the canopy.
- Natural convection within the liquid phase of the PCM is neglected.

When modeling phase change of PCM, especially for the case of thin geometries, neglecting natural convection effects is a practical assumption in literature like the study of Cheng *et al*. (2015) and Xia *et al*. (2017).

The continuity, momentum, and energy equations for air, which governs the transport phenomena inside the container are given below (equations (8)-(11)).

$$\frac{\partial u}{\partial x} + \frac{\partial v}{\partial y} = 0 \qquad (8)$$

$$\rho_f\left(\frac{\partial u}{\partial t} + u\frac{\partial u}{\partial x} + v\frac{\partial u}{\partial y}\right) = -\frac{\partial p}{\partial x} + \mu_f\left(\frac{\partial^2 u}{\partial x^2} + \frac{\partial^2 u}{\partial y^2}\right) \qquad (9)$$

$$\rho_f\left(\frac{\partial v}{\partial t} + u\frac{\partial v}{\partial x} + v\frac{\partial v}{\partial y}\right) = -\frac{\partial p}{\partial y} + \mu_f\left(\frac{\partial^2 v}{\partial x^2} + \frac{\partial^2 v}{\partial y^2}\right) + \rho_f g\beta_T\left(T - T_{ref}\right) \qquad (10)$$

$$\rho_f c_{pf}\left(\frac{\partial T}{\partial t} + u\frac{\partial T}{\partial x} + v\frac{\partial T}{\partial y}\right) = k_f\left(\frac{\partial^2 T}{\partial x^2} + \frac{\partial^2 T}{\partial y^2}\right) \qquad (11)$$

where ρ_f, c_{pf}, k_f, μ_f and β_T are density, specific heat at constant pressure, thermal conductivity, dynamic viscosity, and thermal expansion coefficient of air, respectively. T_{ref} is the minimum temperature in the domain of air.

The reference solution is for polyurethane. Governing equations for PCM plates and polyurethane plates are given below (equations (12)-(15)).

$$C_{PCM\ ap}\frac{\partial T}{\partial t} = k_{PCM}\left(\frac{\partial^2 T}{\partial x^2} + \frac{\partial^2 T}{\partial y^2}\right) \qquad (12)$$

$$C_{PCM\ ap} = \begin{cases} \rho_s c_s & T \le T_s \\ \rho_{PCM}\Delta h\dfrac{\partial \beta}{\partial T} + 0.5\rho_s c_s + 0.5\rho_l c_l & T_s < T < T_l \\ \rho_l c_l & T \ge T_l \end{cases} \qquad (13)$$

$$\beta = \begin{cases} 0 & T \le T_s \\ \dfrac{T - T_s}{T_l - T_s} & T_s < T < T_l \\ 1 & T \ge T_l \end{cases} \qquad (14)$$

$$\rho_{pol}c_{pol}\frac{\partial T}{\partial t} = k_{pol}\left(\frac{\partial^2 T}{\partial x^2} + \frac{\partial^2 T}{\partial y^2}\right) \qquad (15)$$

where Δh is the latent heat, β is the melt fraction, T_s and T_l are solidification and liquefication temperatures, respectively. The subscript ''*s*'' shows the solid phase, and the subscript ''*l*'' shows the liquid phase of PCM. It can be easily seen from equations (12) and (13) that apparent heat capacity method has been applied for the phase change of PCM.

Governing equations have been nondimensionalized by using the following dimensionless variables (equations (16)).

$$x^* = \frac{x}{L} \quad y^* = \frac{y}{L} \quad u^* = \frac{u}{\frac{\alpha_f}{L}} \quad v^* = \frac{v}{\frac{\alpha_f}{L}} \quad p^* = \frac{L^2 p}{\rho_f {\alpha_f}^2} \quad t^* = \frac{\alpha_f t}{L^2} \quad T^* = \frac{T - T_0}{T_H - T_0} \quad {T_s}^* = \frac{T_s - T_0}{T_H - T_0} \quad {T_l}^* = \frac{T_l - T_0}{T_H - T_0} \qquad (16)$$

where T_H (41°C) is the maximum value of the outside air temperature for the investigated time and T_0 is the initial temperature. The initial temperature for the container was selected as 22°C, which is the comfort condition. As the minimum value of the outside air temperature was 23°C, in order not to have minus values for the nondimensional results, we obtained nondimensional energy equations by using initial air temperature value instead of minimum value of the outside air temperature.

Nondimensional forms of initial and boundary conditions for the study are presented in equations (17)-(23).

$$T^*|_{t^*=0} = 0 \qquad (17)$$

$$\left.\frac{\partial T^*}{\partial y^*}\right|_{y^*=0} = 0 \qquad (18)$$

$$u^*|_{on\ walls} = 0 \quad v^*|_{on\ walls} = 0 \qquad (19)$$

$$\frac{\partial T^*}{\partial n^*} = \frac{k_i}{k_f}\frac{\partial T^*}{\partial n^*} \qquad \text{Inside boundary condition} \qquad (20)$$

$$\frac{h_{out}L}{k_f}\left(T^* - {T_{out}}^*\right) = -\frac{k_i}{k_f}\frac{\partial T^*}{\partial n^*} \qquad \text{Outside boundary condition} \qquad (21)$$

i shows PCM or polyurethane

$$\left.\frac{\partial T^*}{\partial x^*}\right|_{x^*=0} = 0 \qquad \text{Symmetry condition for energy equation} \qquad (22)$$

$$\left.\vec{V}^* \cdot \vec{n}^*\right|_{x^*=0} = 0 \qquad \text{Symmetry condition for momentum equations} \qquad (23)$$

Nondimensional forms of the governing equations are given below (equations (24)-(32)).
For air:

$$\frac{\partial u^*}{\partial x^*} + \frac{\partial v^*}{\partial y^*} = 0 \qquad (24)$$

$$\frac{\partial u^*}{\partial t^*} + u^*\frac{\partial u^*}{\partial x^*} + v^*\frac{\partial u^*}{\partial y^*} = -\frac{\partial p^*}{\partial x^*} + Pr\left(\frac{\partial^2 u^*}{\partial x^{*2}} + \frac{\partial^2 u^*}{\partial y^{*2}}\right) \qquad (25)$$

$$\frac{\partial v^*}{\partial t^*} + u^*\frac{\partial v^*}{\partial x^*} + v^*\frac{\partial v^*}{\partial y^*} = -\frac{\partial p^*}{\partial y^*} + Pr\left(\frac{\partial^2 v^*}{\partial x^{*2}} + \frac{\partial^2 v^*}{\partial y^{*2}}\right) + RaPr\left(T^* - {T_{ref}}^*\right) \qquad (26)$$

$$\frac{\partial T^*}{\partial t^*} + u^*\frac{\partial T^*}{\partial x^*} + v^*\frac{\partial T^*}{\partial y^*} = \frac{\partial^2 T^*}{\partial x^{*2}} + \frac{\partial^2 T^*}{\partial y^{*2}} \qquad (27)$$

where Ra is the Rayleigh number, and Pr is the Prandtl number. They are also given below.

$$Ra = \frac{g\beta_T L^3 (T_H - T_0)}{\alpha_f \gamma_f} \qquad (28)$$

$$Pr = \frac{\gamma_f}{\alpha_f} \qquad (29)$$

For PCM and polyurethane plates:

$${C_{PCM\ ap}}^*\frac{\partial T^*}{\partial t^*} = \frac{k_{PCM}}{k_f}\left(\frac{\partial^2 T^*}{\partial x^{*2}} + \frac{\partial^2 T^*}{\partial y^{*2}}\right) \qquad (30)$$

$${C_{PCM\ ap}}^* = \begin{cases} \dfrac{\rho_s c_s}{\rho_f c_f} & T^* \le {T_s}^* \\ \dfrac{\rho_s \Delta h}{(T_l - T_s)\rho_f c_f} + 0.5\dfrac{\rho_s c_s}{\rho_f c_f} + 0.5\dfrac{\rho_l c_l}{\rho_f c_f} & {T_s}^* < T^* < {T_l}^* \\ \dfrac{\rho_l c_l}{\rho_f c_f} & T^* \ge {T_l}^* \end{cases} \qquad (31)$$

$$\frac{\rho_{pol} c_{pol}}{\rho_f c_f}\frac{\partial T^*}{\partial t^*} = \frac{k_{pol}}{k_f}\left(\frac{\partial^2 T^*}{\partial x^{*2}} + \frac{\partial^2 T^*}{\partial y^{*2}}\right) \qquad (32)$$

It can be easily seen that the buoyancy force term $RaPr\left(T^* - {T_{ref}}^*\right)$ plays an important role in the natural convection of air inside the container. Apparent heat capacity method is also obvious in the dimensionless form of the energy equation of PCM.

Solution Method and Mesh Dependency Analysis

In this study, the thermal performance of the container has been investigated for the outside air temperature from 08:00 to 18:00 h on 02.02.2019 in Rio de Janeiro. In other words, thermal performances of PCMs for the time interval, including the hottest time, have been investigated in Rio de Janeiro. Necessary temperature data have been taken from the reference (Internet, 2019). Dimensionless form for the outside air temperature has been obtained, as seen in Fig. 3. Because nondimensional forms of the governing equations have been solved numerically by using COMSOL Multiphysics finite element modeling and simulation software. The function for the dimensionless air temperature has been obtained by Sigma Plot, presented by equation (33), and used in the analysis due to equation (21). It has been observed that the corresponding maximum discrepancy value for dimensional outside temperature is % 4.61. This also corresponds to the temperature difference of 1.43°C.

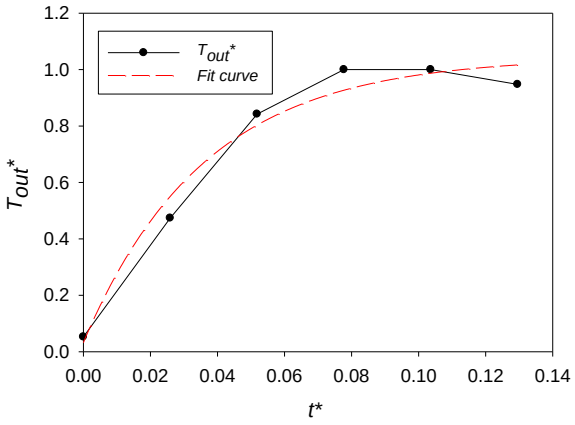

Fig. 3 Dimensionless form of the outside air temperature

$${T_{out}}^* = 0.0318 + 1.0127\left(1 - e^{-27.6841 t^*}\right) \qquad R^2 = 0.9752 \qquad (33)$$

For the calculation of the convection heat transfer coefficient h_{out} for the outside of the container, we assumed that wind is blowing with a speed of 5 m/s (w) along with the container, which is 6 m (L_z) in length. Thermophysical properties of air for the calculation of h_{out} was taken constant at the mean temperature of the outside air, which is 35.67°C, for the investigated time interval. The correlation given in equation (34), which can easily be obtained from the local Nusselt number correlation (Çengel, 2011), has been used for the turbulent external flow outside the container and h_{out} found as 15.37 W/m^{2}K. The value of the h_{out} is also used in equation (21) to get the solution of nondimensional governing equations.

$$\overline{Nu}_L = 0.0385 {Re_L}^{0.8} Pr^{1/3} \quad (34)$$

Mesh dependency analysis was also carried out. The average value of the dimensionless air temperature inside the container depending on dimensionless time was obtained for different number of mesh elements, as seen in Fig. 4. On the other hand, it was observed that the program could not be able to give reasonable results for a mesh with less number of elements than 10633. Mesh with 47742 number of elements was selected by considering the analysis time and accuracy.

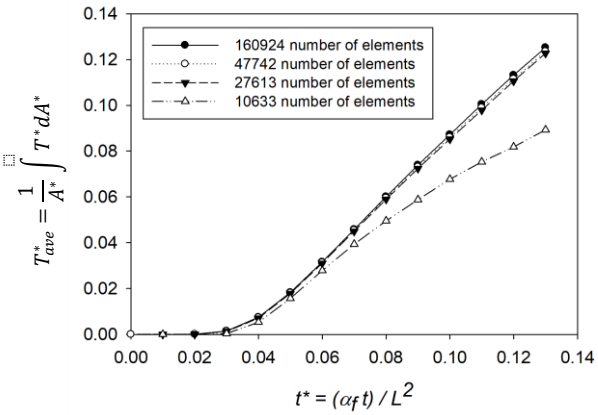

Fig. 4 Dimensionless value of the average temperature of the air for the case of RT 28 HC for different mesh types

Validation of the Code

The code used for the model for fluid inside the container was tested, and results, when steady-state conditions have been reached, are presented in Table 4 for validation. According to this reference model, a square enclosure with a cylinder on its center is considered, as shown in Fig. 5a. The surfaces of the enclosure and cylinder have a constant temperature. Average values of the Nusselt number at the top ($\overline{Nu_T}$), bottom ($\overline{Nu_B}$) and side walls ($\overline{Nu_S}$) are calculated according to equation (35).

$$Nu = \left.\frac{\partial\theta}{\partial n^*}\right|_{wall}, \qquad \overline{Nu} = \int_0^1 Nu\, dS^* \quad (35)$$

where θ is dimensionless temperature, n^* and S^* are the dimensionless length in the normal and horizontal directions to the wall, respectively. On the other hand, validation of code for the fluid has also been performed by comparing numeric results with the time-wise variation of Nusselt numbers due to the problem given in Fig. 5b. In this figure, the square body in the center of the enclosure has the mean temperature of the cold and hot wall temperatures. Time-wise comparisons of the average Nusselt number at the hot bottom wall have been presented in Figs. 6, 7, and 8, respectively for Ra=10^4, Ra=10^5, and Ra=10^6.

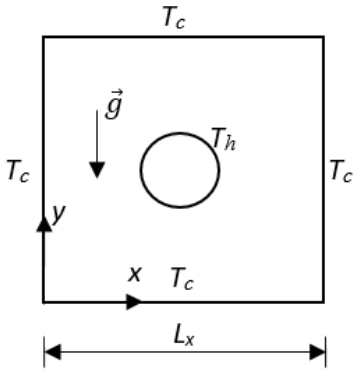

Fig. 5a A square enclosure with a cylinder on its center (for validation with the study of Kim *et al.* (2008))

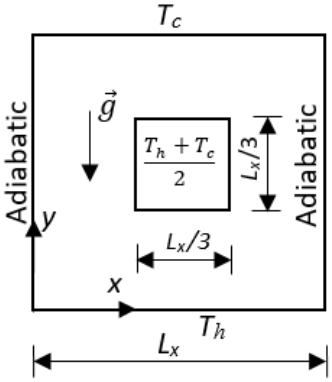

Fig. 5b A square enclosure with a square body on its center (for validation with the study of Ha *et al.* (2002))

Although the study of Kim *et al.* (2008) is time-dependent, flow, and thermal fields reach the steady-state conditions. Because of that reason, Table 4 shows the data at the time when steady-state conditions have been reached. It is expected that reason for the small differences between the results obtained from the numeric code in this study and the results of the study of Kim *et al.* (2008) is due to the difference of mesh and numeric method used. On the other hand, the variations of the average Nusselt numbers at the hot bottom wall are highly compatible with the study of Ha *et al.* (2002), as shown in Figs. 6, 7, and 8.

Table 4 Validation of the model for the fluid code

Ra	$\overline{Nu_S}$	$\overline{Nu_S}$ (Kim *et al.* 2008)	$\overline{Nu_B}$	$\overline{Nu_B}$ (Kim *et al.* 2008)	$\overline{Nu_T}$	$\overline{Nu_T}$ (Kim *et al.* 2008)
10^3	1.5839	1.6947	1.5437	1.6098	1.6261	1.6826
10^4	1.5677	1.7267	1.2444	1.2931	2.0741	2.1822
10^5	2.0571	2.0745	0.4740	0.4780	5.2243	5.4554
10^6	3.6131	3.6646	0.4415	0.3774	10.1355	11.055

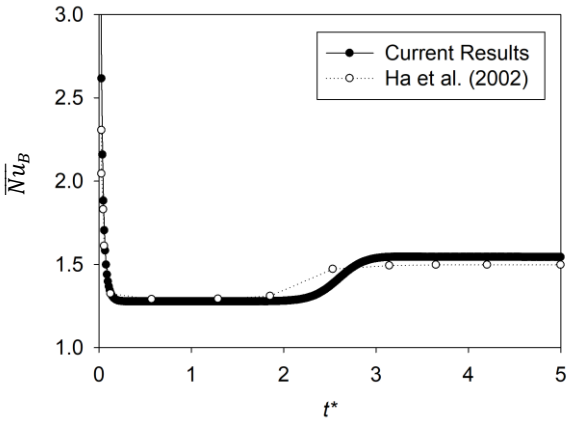

Fig. 6 Time-dependent comparison of the average Nusselt number at the hot bottom wall for Ra=10^4

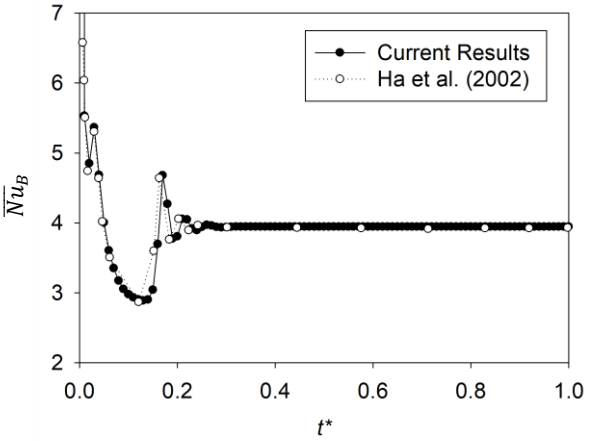

Fig. 7 Time-dependent comparison of the average Nusselt number at the hot bottom wall for Ra=10^5

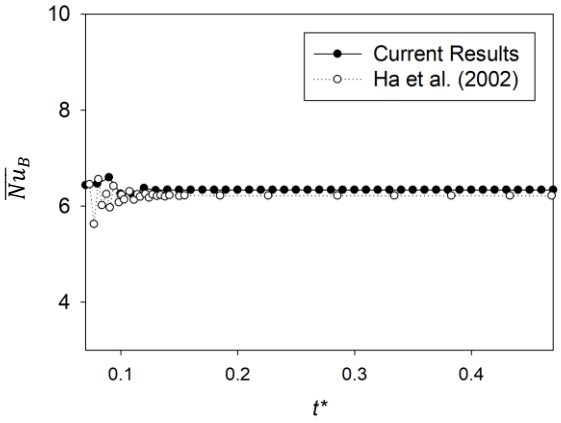

Fig. 8 Time-dependent comparison of the average Nusselt number at the hot bottom wall for Ra=10^6

The code for PCM was also tested for the case of RT 28 HC by using analytical results for freezing in a corner given in the literature as shown in Fig. 9 (Rathjen and Jiji, 1971). The code for phase change is the same both for the solidification and melting process. A square enclosure with 1m length has been considered. It is full of RT 28 HC, which is initially at 305K, and while its two adjacent walls are at a constant temperature of 285K, other walls are isothermal. Corresponding results have been obtained at three different times. It has been observed that the analytical and numerical solidification fronts are almost the same. Dimensional results convenient with the analytical ones have been presented in Fig. 9 for the validation of the PCM code. Because dimensionless equations of terms in the work of Rathjen and Jiji (1971) and this study are different. On the other hand, corresponding dimensionless time values calculated according to equation (16) for a square enclosure with 1 m length have also been given in this figure.

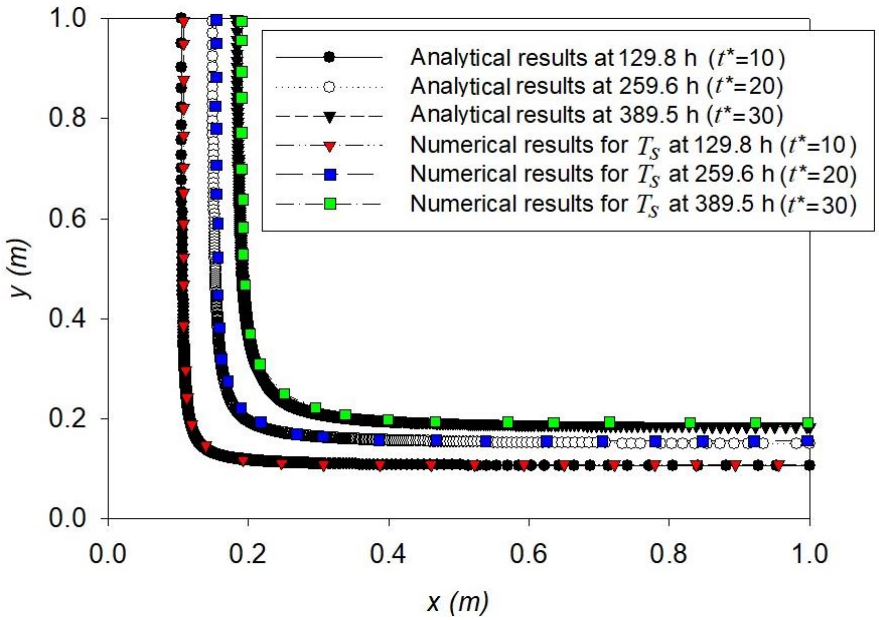

Fig. 9 Validation of the PCM code for the case of RT 28 HC

RESULTS AND DISCUSSION

The dimensionless average temperature values of the air inside the container have been obtained for all the investigated cases, as shown in Fig. 10. It has been observed that the dimensionless average temperature is equal to its initial value for the cases of RT 22 HC and RT 25 HC at the end of the investigation time. On the other hand, this value shows increments of 0.1235 and 0.7710 respect to its initial value, respectively for the cases of RT 28 HC and polyurethane at the end of that time. Corresponding temperature differences with respect to initial or comfort temperature are 2.35°C and 14.65°C, respectively, for the cases of RT 28 HC and polyurethane. One can conclude that the case of RT 28 HC shows better performance when comparing the reference case of polyurethane. The main reason for using PCM is to utilize its latent heat. This causes heat absorption inside the walls and makes the indoor temperature of the container not to rise as in the cases of RT 22 HC and RT 25 HC, or it shows little increment as in the case of RT 28 HC. As there is no heat absorption effect for the polyurethane walls, the average temperature inside the container continues to rise due to the outside hot air. It can be concluded that the usage of PCM reduces the temperature rise within the container; as a result, the need for air conditioning and energy consumption will be reduced by using convenient PCM on the container walls.

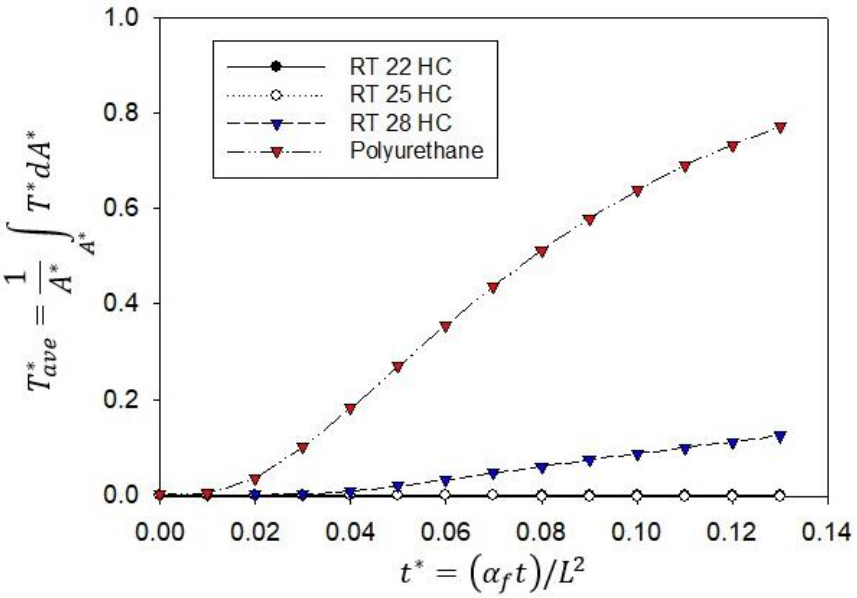

Fig. 10 Average temperature values inside the container ($T^* = \frac{T-T_0}{T_H-T_0}$, T_H = 41°C, T_0 = 22°C)

The places of the melting zone inside the upper, bottom, and sidewalls of the container have been presented in Fig. 11 for all the investigated PCM walls. Red places show the mushy zone. It has been shown that melting starts first for the case of RT 22 HC as its solidification temperature has the lowest value. On the other hand, for the conditions given in this study, the thickness of the mushy zone decreases as the melting temperature of the PCM increases.

Although RT 28 HC has the highest latent heat value, RT 22 HC and RT 25 HC give better performance as their solidification temperatures have lower values, which are close to the initial temperature. The initial temperature for the container was selected as 22°C, and it is greater than the solidification temperature T_s of the RT 22 HC. This means although RT 22 HC is in the form of mushy at the beginning of the process, it shows better cooling performance. In other words, initially, walls with RT 22 HC are mushy and walls with RT 25 HC are about to melt. This means that the heat absorption effect is active. But in the case of walls with RT 28 HC heat absorption effect will be active later. Secondly, as seen in Fig. 11, mushy zone, which absorbs heat, is thinner for the case of RT 28 HC than other cases. These are the reasons why RT 22 HC and RT 25 HC give better performance.

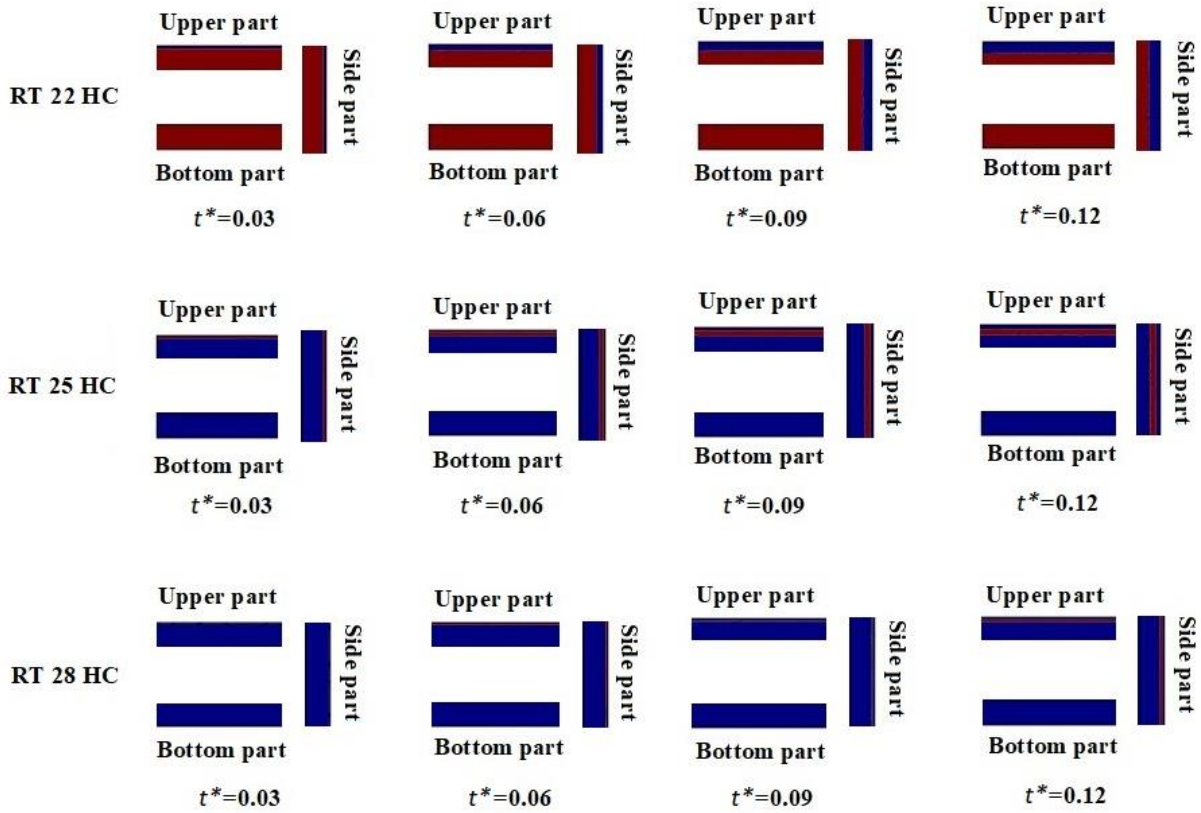

Fig. 11 Melting of the PCM inside the container walls

Table 5 shows the average temperature values of the container parts in dimensionless form for the four investigated cases. Dimensionless average temperature values of T^*_{ave} for each part have been calculated by the dimensionless integral of $\frac{1}{A^*}\int_{A^*} T^* dA^*$. As it has been shown from Table 5, the upper and side parts of the container are almost at the same temperature for the cases of RT 22 HC, RT 25 HC and RT 28 HC. Side parts are generally slightly warmer than upper parts. But for the case of polyurethane walls, the upper part of the container is warmer than side part. According to the results presented in Table 5, one can conclude that RT 25 HC shows better performance by absorbing more heat for the given conditions. The coolest part of the container is the bottom part due to adiabatic condition on this surface. Accordingly, it has been observed that the bottom part of the container is at the initial temperature during the investigation time for the cases of RT 22 HC and RT 25 HC.

Table 5 Average values of dimensionless temperatures of the container parts

t*	**RT 22 HC Upper part** T^*_{ave}	**RT 22 HC Bottom part** T^*_{ave}	**RT 22 HC Side part** T^*_{ave}	**RT 25 HC Upper part** T^*_{ave}	**RT 25 HC Bottom part** T^*_{ave}	**RT 25 HC Side part** T^*_{ave}
0.03	0.020	0	0.021	0.004	0	0.004
0.06	0.074	0	0.078	0.025	0	0.026
0.09	0.136	0	0.142	0.046	0	0.048
0.12	0.193	0	0.202	0.073	0	0.075
t*	**RT 28 HC Upper part** T^*_{ave}	**RT 28 HC Bottom part** T^*_{ave}	**RT 28 HC Side part** T^*_{ave}	**Polyurethane Upper part** T^*_{ave}	**Polyurethane Bottom part** T^*_{ave}	**Polyurethane Side part** T^*_{ave}
0.03	0.078	0	0.080	0.322	0.007	0.305
0.06	0.126	0	0.127	0.632	0.052	0.575
0.09	0.173	0.002	0.174	0.826	0.129	0.752
0.12	0.213	0.003	0.214	0.934	0.217	0.860

During melting process of PCMs inside the walls, Stefan number values for each investigated PCM, which are the ratio of sensible heat to the latent heat, have been presented in Table 6.

Table 6. Stefan numbers for the PCM walls

PCM type	$Ste = \frac{c_l(T_l - T_s)}{\Delta h}$
RT 22 HC	0.03750
RT 25 HC	0.04000
RT 28 HC	0.01818

The temperature and velocity simulations for all the investigated cases are presented in Figs. 12-15. It has been observed that maximum velocity values inside the container increase with time for the cases of RT 22 HC and RT 25 HC. In the case of RT 22 HC, the direction of the airflow inside the container can change. Vortexes take place at the beginning in the case of RT 25 HC, and then clockwise rotation takes place. The direction of the airflow is governed by the buoyancy term of $RaPr\left(T^* - {T_{ref}}^*\right)$ given in equation (26). ${T_{ref}}^*$ is the dimensionless form of the minimum temperature in the domain of air. The investigated phenomenon is time dependent. The term $RaPr\left(T^* - {T_{ref}}^*\right)$ also changes with time on every point of the domain of air. This governs the flow direction. Although it seems there is no temperature difference in the domain of air for the cases of RT 22 HC and RT 25 HC, very little temperature differences in the domain cause the flow to be taken place. ${T_{ref}}^*$ is approximately zero for the cases of PCM walls. This means minimum air temperature is equal to the initial temperature. But in the case of polyurethane walls ${T_{ref}}^*$ has the value of 0.0129, 0.0804, 0.1699 and 0.263 respectively for dimensionless time values of 0.03, 0.06, 0.09 and 0.12. In the cases of RT 22 HC and RT 25 HC, there is no temperature rise has been observed inside the domain of air. In the case of RT 28 HC, the temperature slightly increases with time. As the bottom part of the container is adiabatic, places close to the bottom part in the domain of air are the coldest places. Although polyurethane is used as an isolation material due to its low thermal conductivity value, the temperature inside the container increases rapidly according to other cases in the case of polyurethane walls are used. This presents the fact that making use of the heat sink property of phase change materials for the container walls heals the comfort of the living space. The maximum and minimum values of Rayleigh numbers with the maximum value of dimensionless velocity have been presented in Figs. 12-15. It has also been shown in Figs. 12-15 that, generally, circulation gains strength as a result of velocity magnitude increases with the Rayleigh number. This can easily be seen from Fig.15, where the variation of the maximum Rayleigh number is greater.

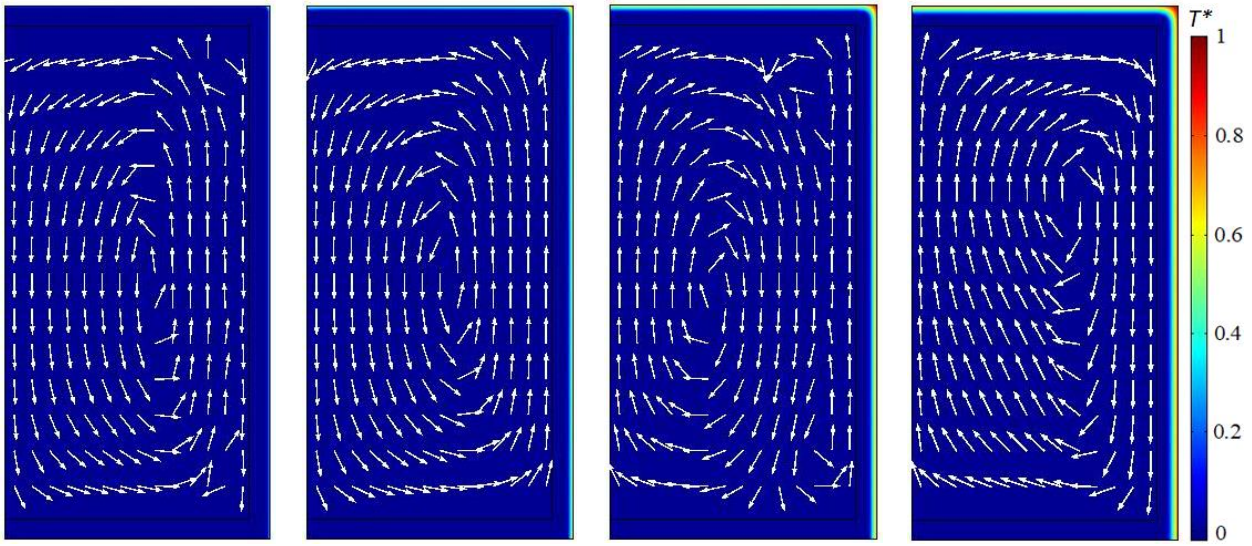

${V^*}_{max}$ =0.31	${V^*}_{max}$ =4.04	${V^*}_{max}$ =12.05	${V^*}_{max}$ =42.72
$Ra_{max} = 2.596 \cdot 10^{10}$	$Ra_{max} = 2.596 \cdot 10^{10}$	$Ra_{max} = 2.596 \cdot 10^{10}$	$Ra_{max} = 2.596 \cdot 10^{10}$
$Ra_{min} = Ra_{max}$	$Ra_{min} = Ra_{max}$	$Ra_{min} = Ra_{max}$	$Ra_{min} = Ra_{max}$
t^*=0.03	t^*=0.06	t^*=0.09	t^*=0.12

Fig. 12 The velocity and temperature simulations inside the container for RT 22 HC

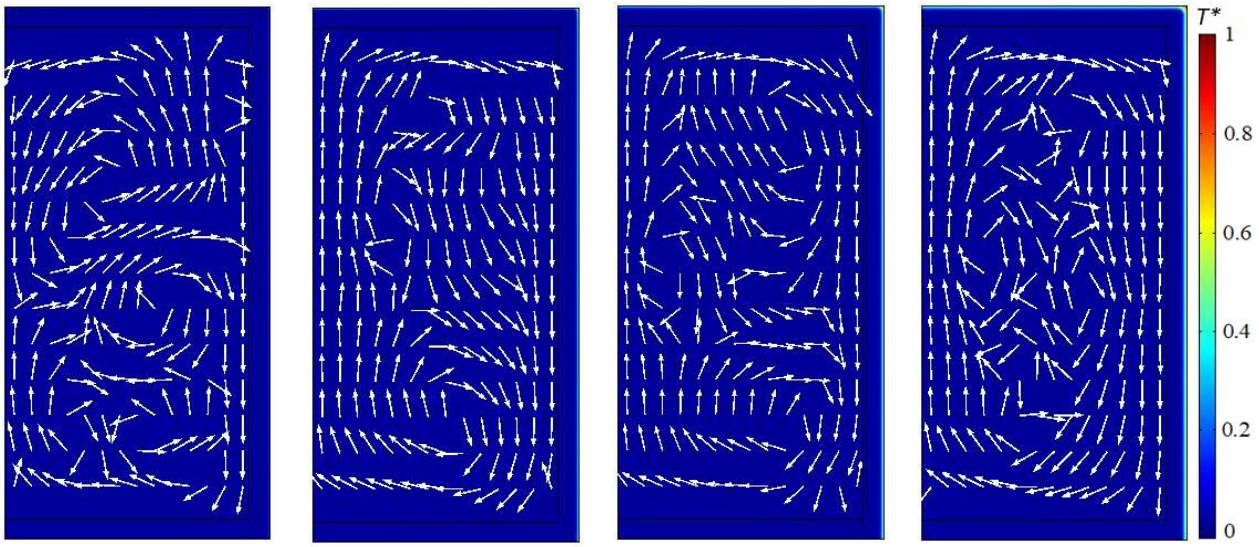

V^*_{max} =1660.61	V^*_{max} =4109.33	V^*_{max} =5478.92	V^*_{max} =5475.16
$Ra_{max} = 2.596 \cdot 10^{10}$	$Ra_{max} = 2.596 \cdot 10^{10}$	$Ra_{max} = 2.597 \cdot 10^{10}$	$Ra_{max} = 2.597 \cdot 10^{10}$
$Ra_{min} \cong Ra_{max}$	$Ra_{min} \cong Ra_{max}$	$Ra_{min} = 2.596 \cdot 10^{10}$	$Ra_{min} = 2.596 \cdot 10^{10}$
t^*=0.03	t^*=0.06	t^*=0.09	t^*=0.12

Fig. 13 The velocity and temperature simulations inside the container for RT 25 HC

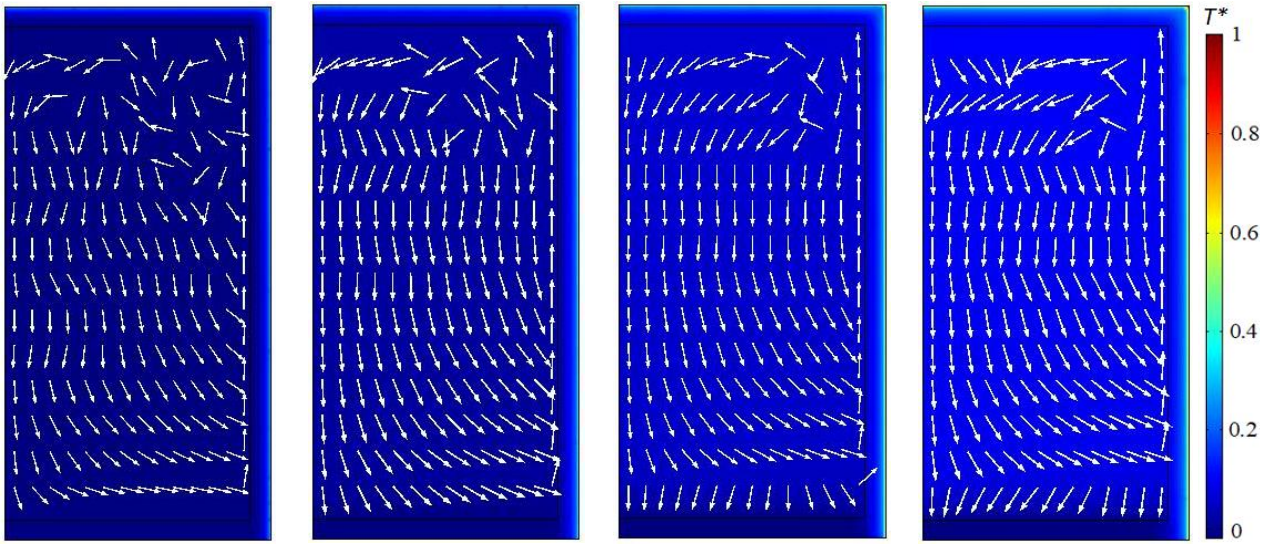

V^*_{max} =2524.41	V^*_{max} =3780.90	V^*_{max} =3420.69	V^*_{max} =3246.54
$Ra_{max} = 2.596 \cdot 10^{10}$	$Ra_{max} = 2.596 \cdot 10^{10}$	$Ra_{max} = 2.596 \cdot 10^{10}$	$Ra_{max} = 2.595 \cdot 10^{10}$
$Ra_{min} = 2.595 \cdot 10^{10}$	$Ra_{min} = 2.587 \cdot 10^{10}$	$Ra_{min} = 2.579 \cdot 10^{10}$	$Ra_{min} = 2.572 \cdot 10^{10}$
t^*=0.03	t^*=0.06	t^*=0.09	t^*=0.12

Fig. 14 The velocity and temperature simulations inside the container for RT 28 HC

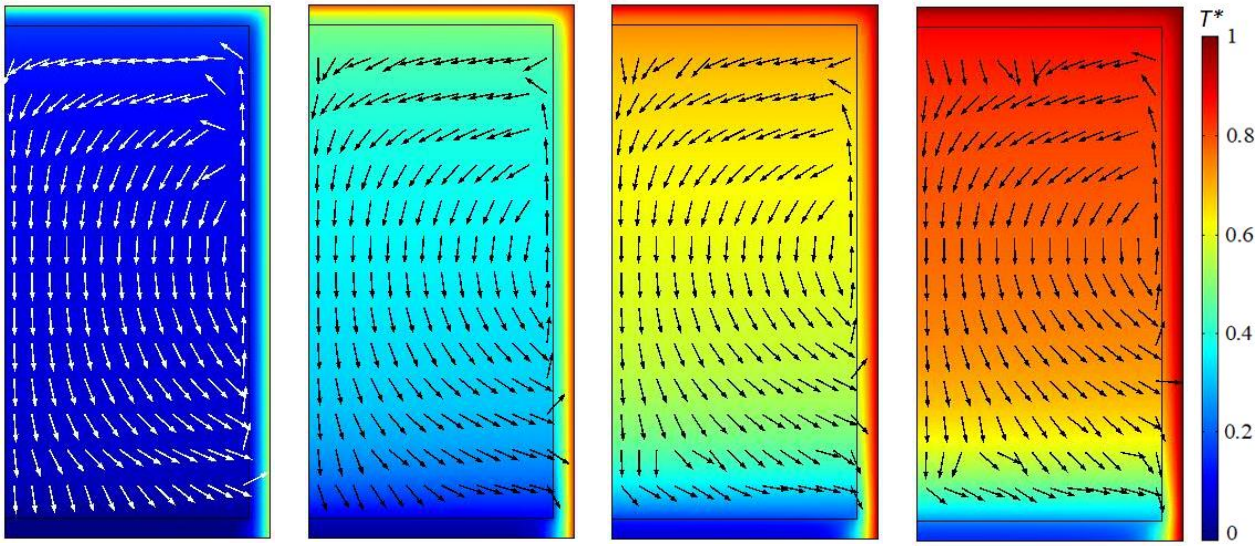

V^*_{max} =5168.10
$Ra_{max} = 2.594 \cdot 10^{10}$
$Ra_{min} = 2.561 \cdot 10^{10}$
t^*=0.03

V^*_{max} =3700.29
$Ra_{max} = 2.583 \cdot 10^{10}$
$Ra_{min} = 2.508 \cdot 10^{10}$
t^*=0.06

V^*_{max} =2550.80
$Ra_{max} = 2.568 \cdot 10^{10}$
$Ra_{min} = 2.473 \cdot 10^{10}$
t^*=0.09

V^*_{max} =2145.90
$Ra_{max} = 2.553 \cdot 10^{10}$
$Ra_{min} = 2.453 \cdot 10^{10}$
t^*=0.12

Fig. 15 The velocity and temperature simulations inside the container for polyurethane

Biot numbers have been calculated for the upper and side parts of the container. These parts are also in contact with the hot outside air, and as a result, the temperature gradients inside these parts are greater. Equations (36) and (37) have been used for the calculation of Biot numbers, respectively, for the upper and side parts of the container. As it is well known from the definition of the Biot number, the following equations show the rate of convection on the body to the conduction inside the body. Because convection on the body is equal to the conduction of fluid on the surface of the body.

Variation of the Biot numbers for the investigated cases are presented in Table 7. It can easily be observed from this table that heat absorption due to the phase change of PCM causes the Biot numbers to decrease. In other words, Biot number values are zero for the cases of RT 22 HC and RT 25 HC and approximately zero for the case of RT 28 HC. On the other hand, Biot numbers for the polyurethane parts increase with time. It has also been observed from Table 7 that Biot number decreases after melting starts and plays an important role to show the heat absorption effect for the case of RT 28 HC.

$$Bi_{upper} = \frac{k_f}{k_{\substack{PCM\ or \\ Polyurethane}}} \frac{\left(\frac{1}{S^*}\int_{S^*}\frac{\partial T^*}{\partial y^*}dS^*\right)_{\substack{on\ the \\ surface\ contact \\ with\ inside\ air}}}{\left(\frac{1}{S^*}\int_{S^*}\frac{\partial T^*}{\partial y^*}dS^*\right)_{\substack{on\ the \\ surface\ contact \\ with\ outside\ air}}} \quad (36)$$

$$Bi_{side} = \frac{k_f}{k_{\substack{PCM\ or \\ Polyurethane}}} \frac{\left(\frac{1}{S^*}\int_{S^*}\frac{\partial T^*}{\partial x^*}dS^*\right)_{\substack{on\ the \\ surface\ contact \\ with\ inside\ air}}}{\left(\frac{1}{S^*}\int_{S^*}\frac{\partial T^*}{\partial x^*}dS^*\right)_{\substack{on\ the \\ surface\ contact \\ with\ outside\ air}}} \quad (37)$$

Table 7 Variation of Biot numbers for the upper and side parts of the container

Container Part	t^* = 0.03	t^* = 0.06	t^* = 0.09	t^* = 0.12
Upper PCM (RT 22 HC)	0	0	0	0
Side PCM (RT 22 HC)	0	0	0	0
Upper PCM (RT 25 HC)	0	0	0	0
Side PCM (RT 25 HC)	0	0	0	0
Upper PCM (RT 28 HC)	0.001	0.001	0	0
Side PCM (RT 28 HC)	0.001	0.003	0.002	0.002
Upper Polyurethane	0.064	0.101	0.128	0.152
Side Polyurethane	0.217	0.336	0.414	0.485

CONCLUSION

In this study, the thermal comfort of the container has been investigated for three different types of PCMs and polyurethane walls for the hot summer day in Rio de Janeiro. Numeric analyses for 10 hours show that the best cooling effect due to the melting of PCM has been observed for the cases of RT 22 HC and RT 25 HC. Although RT 28 HC has the highest latent heat, the

temperature of the air inside the container slightly increases for that case as its solidification temperature is not close to the initial temperature, unlike other investigated PCMs. It has also been observed that although the thermal conductivity value of polyurethane is much lower than these of investigated PCMs, using isolation materials like polyurethane does not ensure thermal comfort like PCMs. It has been concluded from this study that making use of the heat absorption ability of PCMs during melting presents considerably better performance on the thermal comfort inside the living area.

In this study, the superiority of using convenient PCMs for the thermal comfort of the container has been demonstrated. On the other hand, this study presents dimensionless process of phenomena with phase change of PCMs on the container walls and natural convection inside the container. Because nondimensionalization is a practical and useful approach.

This study also shows that utilizing the convenient PCMs on the container or building walls will reduce the energy consumption in the world where energy demand increases continuously.

REFERENCES

Arce E., Agrawal R., Suárez A., Febrero L. and Luhrs C. C., 2020, Modeling of Energy Demand and Savings Associated with the Use of Epoxy-Phase Change Material Formulations, *Materials*, 13(3), 639, 1-15.

Álvarez S., Cabeza L. F., Ruiz-Pardo A., Castell A. and Tenorio J. A., 2013, Building Integration of PCM for Natural Cooling of Buildings, *Appl. Energ.*, 109, 514–522.

Beltrán R. D. and Martínez-Gómez J., 2019, Analysis of Phase Change Materials (PCM) for Building Wallboards Based on the Effect of Environment, *Journal of Building Engineering*, 24, 1-16, 100726.

BING, 2019, BING Federation of European Rigid Polyurethane Foam Association, *Thermal Insulation Materials Made of Rigid Polyurethane Foam (PUR/PIR)- Properties – Manufacture*, *Report No:1 (October 2006)*, Av. E. Van Nieuwenhuyse 6, 1160 Brussels-Belgium.
http://highperformanceinsulation.eu/wp-content/uploads/2016/08/Thermal_insulation_materials_made_of_rigid_polyurethane_foam.pdf.

Cheng W., Xie B., Zhang R., Xu Z. and Xia Y., 2015, Effect of Thermal Conductivities of Shape Stabilized PCM on Under-Floor Heating System, *Appl. Energ.*, 144, 10–18.

Chou H. M., Chen C. R. and Nguyen V. L., 2013, A New Design of Metal-Sheet Cool Roof Using PCM, *Energ. Buildings*, 57, 42–50.

Çengel Y. A., Cimbala J. M., 2005, *Fluid Mechanics - Fundamentals and Applications* (First Ed.), *McGrawHill*, New York.

Çengel Y. A., 2011, *Isı ve Kütle Transferi – Pratik Bir Yaklaşım* (Third Ed.), *Güven Bilimsel*, İzmir.

Derradji L., Errebai F. B. and Amara M., 2017, Effect of PCM in Improving the Thermal Comfort in Buildings, *Enrgy. Proced.*, 107, 157 – 161.

Elarga H., Fantucci S., Serra V., Zecchin R. and Benini E., 2017, Experimental and Numerical Analyses on Thermal Performance of Different Typologies of PCMs Integrated in the Roof Space, *Energ. Buildings*, 150, 546–557.

Gracia A., Navarro L., Castell A., Ruiz-Pardo A., Álvarez S. and Cabeza L. F., 2013, Thermal Analysis of a Ventilated Facade with PCM for Cooling Applications, *Energ. Buildings*, 65, 508–515.

Ha M. Y., Kim I. K., Yoon H. S., Yoon K. S. and Lee J. R., 2002, Two-Dimensional and Unsteady Natural Convection in a Horizontal Enclosure with a Square Body, *Numer Heat Tr A-Appl*, 41:183-210.

Hichem N., Noureddine S., Nadia S. and Djamila D., 2013, Experimental and Numerical Study of a Usual Brick Filled with PCM to Improve the Thermal Inertia of Buildings, *Enrgy. Proced*., 36, 766 – 775.

Hu Y., Heiselberg P. K. and Guo R., 2020, Ventilation Cooling/Heating Performance of a PCM Enhanced Ventilated Window - An Experimental Study, *Energ. Buildings*, 214, 109903, 1-12.

Internet, 2019, Previsao do tempo.
https://www.climatempo.com.br/previsao-do-tempo/cidade/321/riodejaneiro-rj.

Kharbouch Y., Mimet A. and Ganaoui M. E., 2017, A Simulation Based-Optimization Method for Energy Efficiency of a Multi-Zone House Integrated PCM, *Enrgy. Proced*., 139, 450-455.

Kim B. S., Lee D. S., Ha M. Y. and Yoon H. S., 2008, A Numerical Study of Natural Convection in a Square Enclosure with Circular Cylinder at Different Vertical Locations, *Int. J. Heat Mass Tran.*, 51, 1888-1906.

Li S., Zhu N., Hu P., Lei F. and Deng R., 2019, Numerical Study on Thermal Performance of PCM Trombe Wall. *Enrgy. Proced*., 158, 2441-2447.

Meng E., Yu H. and Zhou B., 2017, Study of the Thermal Behavior of the Composite Phase Change

Material (PCM) Room in Summer and Winter, *Appl. Therm. Eng.*, 126, 212–225.

Park B, Cho J. and Jeong Y., 2019, Thermal Performance Assessment of Flexible Modular Housing Units for Energy Independence Following Disasters, *Sustainability*, 11(20), 5561, 1-17.

Rathjen K. A. and Jiji L. M., 1971, Heat Conduction with Melting or Freezing in a Corner, *J. Heat Transf.*, 93(1), 101-109.

Rubitherm, 2019a, Rubitherm Phase Change Material, *Applications*, https://www.rubitherm.eu/en/applications.html.

Rubitherm, 2019b, Rubitherm Phase Change Material, *PCM RT-Line*, https://www.rubitherm.eu/en/index.php/productcategory/organische-pcm-rt.

Shobo A. B., Mawire A. and Aucamp M., 2018, Rapid Thermal Cycling of Three Phase Change Materials (PCMs) for Cooking Applications, *J. Braz. Soc. Mech. Sci.*, 40:329, 1-12.

Stritih U., Tyagi V. V., Stropnik R., Paksoy H., Haghighat F., and Mastani Joybari M, 2018, Integration of Passive PCM Technologies for Net-Zero Energy Buildings, *Sustain. Cities Soc*., 41, 286–295.

Udosen A. N., 2019, Numerical Study of High Density Polyethylene–PCM Capsules for Passive Cooling Application in Intermodal Steel Building Space Envelope, *Nigerian Journal of Technology*, 38 (2), 384-398.

Ulloa C., Arce M. E., Rey G., Miguez J. L. and Hernandez J., 2017, Recycling COR-TEN Sea Containers into Service Modules for Milirary Applications: Thermal Analysis, *Energies*, 10(6):820, 1-13.

Wang J., Long E., Qin W. and Xu L., 2013, Ultrathin Envelope Thermal Performance Improvement of Prefab House by Integrating with Phase Change Material. *Energy. Buildings*, 67, 210–216.

Xia X., Meng E., Chen Y., Liu Y., Chen Q., Lu Y. and Chen J., 2017, Numerical Study of the Thermal Performance of the PCM Wall Under Periodical Outside Temperature Waves, *Procedia Engineer*., 205, 3478–3484.

Ye R., Lin W., Yuan K., Fang X. and Zhang Z., 2017, Experimental and Numerical Investigation on the Thermal Performance of Building Plane Containing $CaCa_2.6H_2O$/Expanded Graphite Composite Phase Change Material. *Appl. Energ*., 193, 325-335.

Zalba B., Marin J. M., Cabeza L.F. and Mehling H., 2003, Review on Thermal Energy Storage with Phase Change: Materials, Heat Transfer Analysis and Applications, *Appl. Therm. Eng.*, 23,251–283.

Çiğdem SUSANTEZ graduated from the Mechanical Engineering Department of Trakya University in 2007 with the highest degree in faculty. She received her PhD degree in 2015 from Trakya University. She has been working as an Instructor Dr. at Mechanical Engineering Department of Trakya University. Her main research fields are genetic algorithms, fluid mechanics, heat and mass transfer, nanofluids and phase change materials.

Aldélio Bueno CALDEIRA graduated Cum Laude in Mechanical Engineering in 1995 and received his DSc degree from Federal University of Rio de Janeiro in 2004. He works in Brazilian Army since 1997 and he is military professor of Mechanical Engineering at Military Institute of Engineering (IME) since 2004. His main research fields are heat transfer, combustion, aerodynamics, optimisation and inverse problems.